Hindawi
International Journal of Photoenergy
Volume 2023, Article ID 2493231, 9 pages
https://doi.org/10.1155/2023/2493231

Research Article

Coprecipitation Methodology Synthesis of Cobalt-Oxide Nanomaterials Influenced by pH Conditions: Opportunities in Optoelectronic Applications

V. Ratchagar,[1] M. Muralidharan,[2] M. Silambarasan,[3] K. Jagannathan,[4] P. Kamaraj,[5] Suresh Kumar Subbiah,[6] P. A. Vivekanand,[7] Govindasami Periyasami,[8] Mostafizur Rahaman,[8] Perumal Karthikeyan,[9] and Girma Gonfa[10]

[1]*Department of Physics, Theivanai Ammal College for Women (Autonomous), Villupuram 605602, India*
[2]*Department of Materials Science, Guindy Campus, University of Madras, Chennai 600025, India*
[3]*Department of Physics, Saveetha Engineering College, Chennai 602105, India*
[4]*Department of Physics, SRM Institute of Science and Technology, Vadapalani, Chennai 600026, India*
[5]*Department of Chemistry, Bharath Institute of Higher Education and Research, Chennai 600073, India*
[6]*Centre for Materials Engineering and Regenerative Medicine, Bharath Institute of Higher Education and Research, Chennai 600073, TN, India*
[7]*Centre for Catalysis Research and Department of Chemistry, Saveetha Engineering College, Chennai 602105, India*
[8]*Department of Chemistry, College of Science, King Saud University, P.O. Box 2455, Riyadh 11451, Saudi Arabia*
[9]*Department of Chemistry and Biochemistry, Ohio State University, 170A CBEC, 151 Woodruff Avenue, Columbus, Ohio 43210, USA*
[10]*Department of Chemical Engineering, Addis Ababa Science and Technology University, 16417 Addis Ababa, Ethiopia*

Correspondence should be addressed to K. Jagannathan; researcherscience7@gmail.com, P. Kamaraj; kamaraj97@yahoo.co.in, and Girma Gonfa; kiyaagonfaa@gmail.com

Received 27 January 2023; Revised 29 May 2023; Accepted 15 June 2023; Published 11 July 2023

Academic Editor: Umapada Pal

The cobalt oxide (Co_3O_4) nanomaterials were prepared by coprecipitation synthesis technique by maintaining the pH of the mother solution at 7, 8, and 9. The prepared nanomaterials were subjected to structural and optical characterizations, and the results were examined. The optical absorption spectral studies reveal that the two absorption bands indicate ligand–metal coordination. The photoluminescence spectra contain emission peak at 488 and 745 nm due to size and shape of the synthesized materials. The magnetic nature of the samples was identified from the hysteresis loop traced by vibrating sample magnetometry (VSM). The Fourier transform infrared (FT-IR) spectrum of Co_3O_4 nanomaterials reveals two sharp bands absorbed in 584 and 666 cm^{-1}. This ascribes to the Co-O and O-Co-O stretching, respectively. As the pH of the solution varied from 7 to 10, the SEM image authenticates the transformation of Co_3O_4 nanomaterials morphology from spherical to cubic to agglomerated shape. From the UV-Vis spectra, two absorption bands around 473 nm and 762 nm are observed for the materials prepared at pH 7 and 8. But at pH 9, these two peaks were shifted towards higher wavelengths 515 nm and 777 nm. The observed ferromagnetic nature of Co_3O_4 nanomaterials clearly show the role of surface spins and surface morphology on the magnetic properties of Co_3O_4 nanomaterials. The cyclic voltammetry (CV) curves show the rectangular type of voltammogram. This is an indication of good charge propagation with the electrodes. The Nyquist plots of Co_3O_4 nanomaterials have a semicircle in the high frequency region and a vertical line in the low frequency region. The results suggest that Co_3O_4 is found to be a promising material for the fabrication of light-emitting diodes, solar cells, and optoelectronic devices.

1. Introduction

The nanosized semiconducting compounds have been attracting researcher's interest due to their structural, chemical, physical, optical, and magnetic properties which differ from their bulk counterparts [1]. P-type semiconductor such as cobalt oxide (Co_3O_4) nanomaterials have been attracting attentions due to their excellent properties [2, 3]. Cobalt oxide has been widely investigated for various applications such as sensors, electrochromic devices, and catalysts and lithium batteries [4, 5]. Cobalt oxide shows interesting optical, magnetic, and electrochemical properties when it is reduced to the nanometer scale [6]. It has a wide range of morphological structures, such as nanorods, core shells, nanowires, helixes, nanobelts, nanoplatelets, and nanotubes with a surface-to-volume ratio [7]. There are various synthesis methods that have been employed to synthesis Co_3O_4 nanomaterials via physical deposition, wet-chemical, and thermal route [8].

In the synthesis of metal oxide nanoparticles via the hydrothermal method, the pH of the solution significantly affects the purities, morphology, and structure of the nanoparticles. For instance, Bi_2O_3 nanomaterials synthesised at pH of 13 show a pure monoclinic phase with a higher degree crystalline compared to the nanomaterials prepared at pH 11 and 12 [9]. In the case of ZrO_2-based nanomaterial, the pH of the reaction solution at 7, 8, and 9 provides ZrO_2 with good crystalline nature [10]. The ZrO_2 crystal sizes were 12, 14, and 16 nm for pH 7, 8, and 9, respectively [10]. Moreover, the ZrO_2 prepared at pH 7 exhibited a ferromagnetic nature against the diamagnetic nature that exhibited by the materials prepared at pH 8 and 9 [10]. Similarly, in the case of SnO_2 nanomaterials synthesized by microwave-assisted method, the morphology changes (change in spherical shape to flower shape) when the pH varied from 7 to 9 [11]. Moreover, the magnetic behaviour changes from ferromagnetic to diamagnetic nature [11]. Many parameters exhibit favourable changes when pH was varied including physical, chemical, magnetic, and optical properties (energy gap, crystal structure, and luminescence). Hence, many works consider the effect of pH during the preparation and characterisation of nanomaterials using chemical methods [12].

Hence, the present work is focused on the synthesis of Co_3O_4 nanomaterials by the coprecipitation method and studying the effect of pH on the structural, morphological, and physical properties of Co_3O_4 nanomaterials. Finally, the chromaticity parameters of the Co_3O_4 nanomaterial were evaluated.

2. Experimental

2.1. Materials

2.1.1. Cobalt Oxide Nanomaterial Preparation. In general, the cobalt chloride solution was mixed with various concentrations of ammonia solutions, and the resulting product was calcinated. In this work, three samples were prepared by maintaining the pH of the reaction solution at 7, 8, and 9. Typically, a 0.1 mol of cobalt chloride (Sigma-Aldrich ≥98%) solution was prepared by adding 50 ml of demineralised water (solution A). Then, 20 ml of ammonium hydroxide (~28% NH_3 base, Sigma-Aldrich) solution was added to 30 ml of dematerialized water (solution B). The solutions A and B were mixed and stirred for 30 minutes. In this reaction, the ammonia (NH_4OH) solution was added to maintain the required pH. The final solution was stirred for 6 h. The obtained precipitate was washed using ethanol and deionised water consequently. Then, the washed material was dried at 80°C for 12 h in a hot air oven. It was calcined at 500°C for 5 h. The ammonium hydroxide concentration is modified based on the pH values in the required solution B.

2.1.2. Materials Characterisation. The powder XRD patterns were recorded for the prepared samples in the Xpert high score instrument over the 2θ range of 20°-80° in steps of 0.02°. From these patterns, information regarding particle size and defects was obtained. The FT-IR spectrum was recorded using Avatar 330, in the wavelength range 400–4000 cm^{-1}. The KBr pellet technique was used. The spectrum can be used to identify and differentiate molecules present in the sample. The synthesized powder was analysed by the FEI Quanta FEG 200-High Resolution Scanning Electron Microscope. SEM is employed to study the crystal structure and morphology of the samples. The UV-Vis absorption spectra of the synthesized materials were recorded from 190 nm to 1100 nm using a Shimadzu spectrophotometer.

It is employed for the quantitative analysis of samples. The photoluminescence responses of the samples were examined using a Jobin Yvon FLUOROLOG-FL3-11 spectrophotometer under an excitation wavelength of 330 nm. It arises when the emitting excited state is generated by the absorption of a photon. The Lake Shore vibrating sample magnetometer (model 7404) was used to study the magnetic properties of synthesized nanomaterials. The colour coordinates of the prepared samples were investigated within the framework of CIE 1931. The electrochemical performance of Co_3O_4 nanomaterials was evaluated using cyclic voltammetry (CV) and electrochemical impedance spectroscopy (EIS) (three electrode system). The working electrode was made with active material Co_3O_4 (80 wt. %); active carbon black (10 wt. %) and polyvinylidene fluoride (10 wt. %). The slurry was coated in the stainless steel which is the current collector. The different scan rates of 10, 20, 30, 50, and 100 mVs^{-1} and the potential window of -0.2 to 1 V were used for the measurement. In this experiment, a 1 M KOH solution was used as an electrolyte.

3. Results and Discussion

3.1. XRD Analysis. The X-ray powder diffraction (XRD) patterns of the synthesised Co_3O_4 nanomaterials and JCPDS used for comparison are depicted in Figure 1. Figure 1(a) represents the X-ray powder diffraction

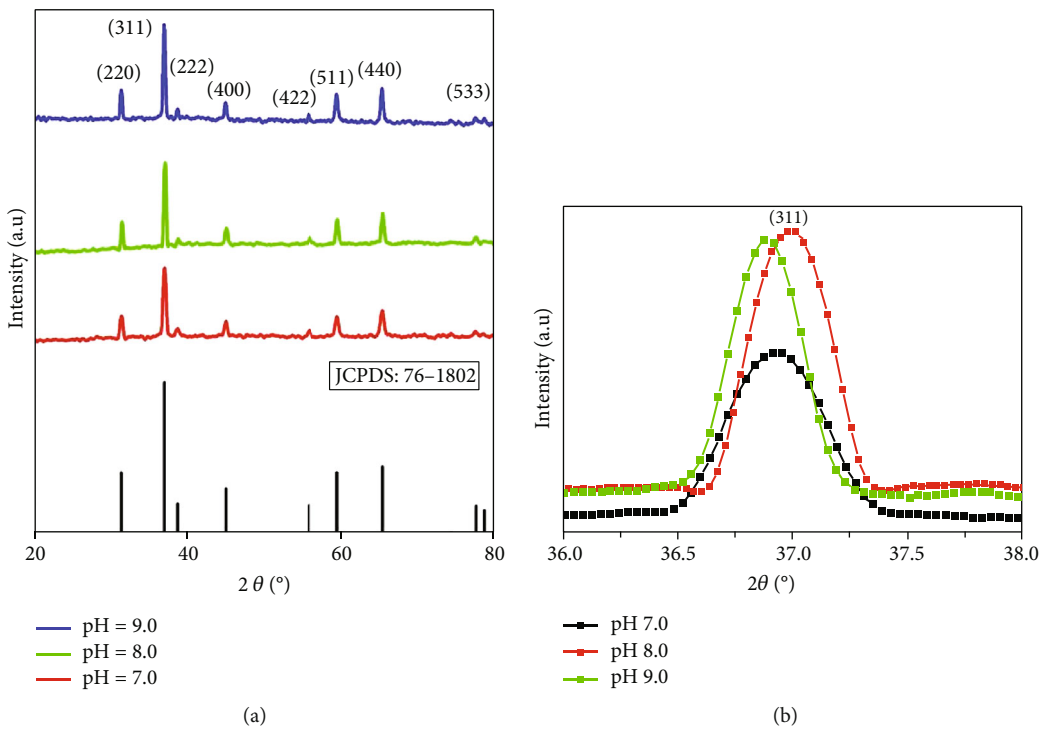

Figure 1: X-ray diffraction and peak diffraction for Co_3O_4 nanoparticles. (a) Ray diffraction (XRD) pattern and (b) diffraction peak.

(XRD) patterns of the prepared samples. All the peaks coincided with JCPDS file no. 76-1802, which suggests a cubic spinel structure with space group Fd3m [13]. The intensity of the prepared Co_3O_4 nanomaterial increases, while increasing pH which suggests that the prepared materials are of good crystalline nature. This was further confirmed by the variation in crystallite size, calculated from the Scherrer equation

$$D = \frac{K\lambda}{\beta \mathrm{COS}\theta}, \quad (1)$$

where D is the crystallite size, λ is the X-ray wavelength (CuK_α – 1.5406 Å), β is the FWHM, and θ is the diffraction angle. The calculated crystal sizes reduce from 14 to 10 nm, while the pH changes from 7 to 9. The diffraction peak shifted slightly from right to left while increasing pH of the solution (Figure 1(b)). This is due to the different pH of the reaction solution providing energy to molecules to occupy the proper equilibrium sites, resulting in the improvement of the crystalline property and degree of orientation of the Co_3O_4 nanomaterials.

3.2. Fourier Transform Infrared Spectroscopy. FTIR spectroscopic analysis done to determine the functional group characters and purity of synthesized metal oxide nanoparticles. From Figure 2, two major sharp bands observed at 584 cm^{-1} and 666 cm^{-1} which ascribes the symmetric stretches to Co-O [14] and O-Co-O [15], respectively. The broad bands at 3300 cm^{-1} are attributed to the O-H stretching. The weak IR band at 1652 and 1619 cm^{-1} accounting as symmetric and

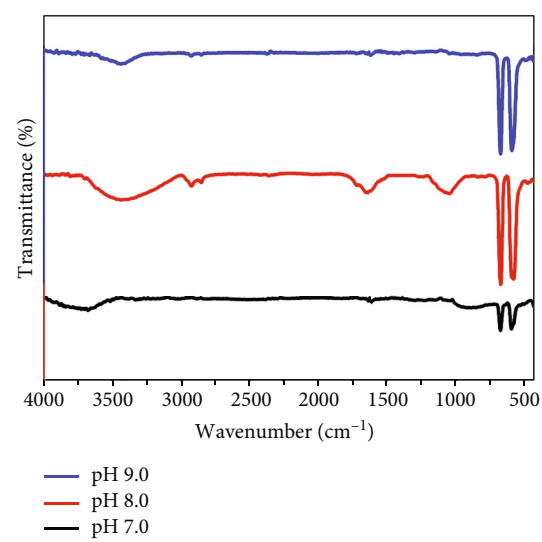

Figure 2: FTIR Spectrum of Co_3O_4 nanomaterials.

asymmetric stretching of H-O-H because due to the adsorption of moisture. These OH and H-O-H moisture bands may be observed due to the sample pellets being exposed in air ambiance.

3.3. Morphology Studies. Figure 3 shows the scanning electron microscope (SEM) images of synthesized nanomaterials. The particles are of uniform size and well-defined spherical shapes. Moreover, when the pH of the solution was increased, the shapes of the particles are growing in

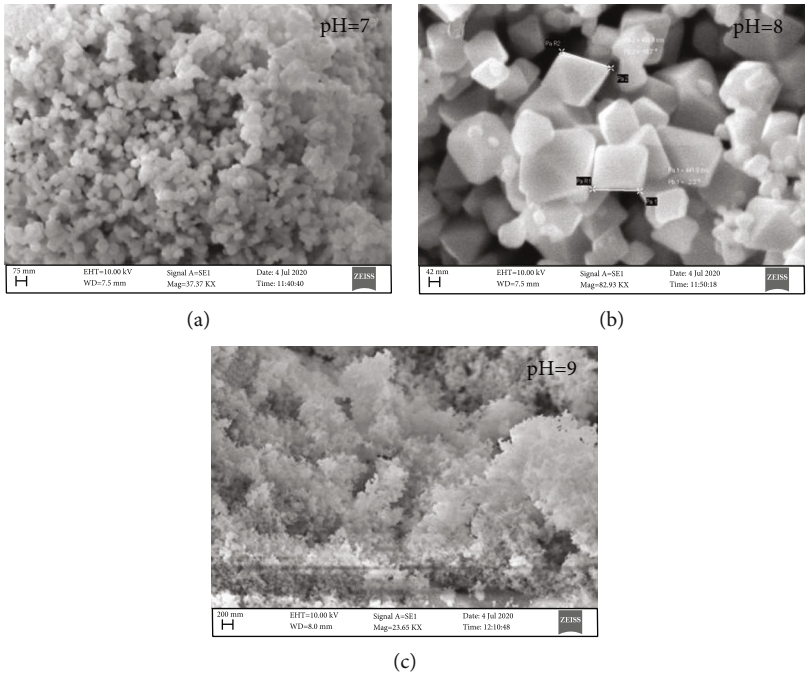

Figure 3: Scanning electron microscopy (SEM) image of Co_3O_4 nanoparticles (a) at pH 7.0 (b), at pH 8.0 and (c) at pH 9.0.

certain direction such as spherical and cubic (Figure 3(a)) to the regular shape of the cubic structure (Figure 3(b)). Figure 3(c) shows the agglomerated, spherical-shaped particles. Here, the pH of the solution plays a major role in the formation of nucleation sites which determine the shape of the particles. The other reason for such morphological change might be due to the presence of OH^- ions in the precursor solution that creates noncovalent bonding interaction. This intermolecular interaction during the reaction is often referred to as the steric effect, which leads to the raising of repulsive forces between overlapping electron clouds. So, it authenticates the transformation from spherical to cubic to agglomerated shape.

3.4. UV-Vis Spectra and Optical Bandgap. The UV-Vis spectra of the solutions were measured using a UV-Vis spectrophotometer (Lambda 25, Perkin Elmer Inc., Shelton, CT, USA) from 200 nm to 1200 nm in 10 mm quartz cuvettes at room temperature, and ε are given in $M^{-1}\,cm^{-1}$. Figure 4 shows the optical absorption spectra of synthesized materials. There are two absorption bands around 473 nm and 762 nm observed for the materials prepared at pH 7 and 8, respectively. But at pH 9, these two peaks were shifted towards higher wavelength such as 515 nm and 777 nm, respectively. These two absorption bands are associated with the O^{2-}-to-Co^{2+} and O^{2-}-to-Co^{3+} charge transfer processes in the Co_3O_4 nanomaterials. The peak at 276 nm fits the bonding-antibonding nature of the $(\pi - \pi^*)$ electronic transition between cobalt and oxygen [16]. The band gaps were calculated as 2.5, 2.4, and 2.2 eV for the materials prepared at pH 7, 8, and 9, respectively. Figure 5 shows the optical bandgap of Co_3O_4 nanomaterials. These E_g values are associated with $O_2^- \rightarrow Co^{3+}$ and $O_2^- \rightarrow Co^{2+}$ its charge transfer process unit. The calculated band gap value is low compare to the bulk value of Co_3O_4 (3.17 eV). The band gap decreases due to the crystal size effects of Co_3O_4 nanomaterials [17–20].

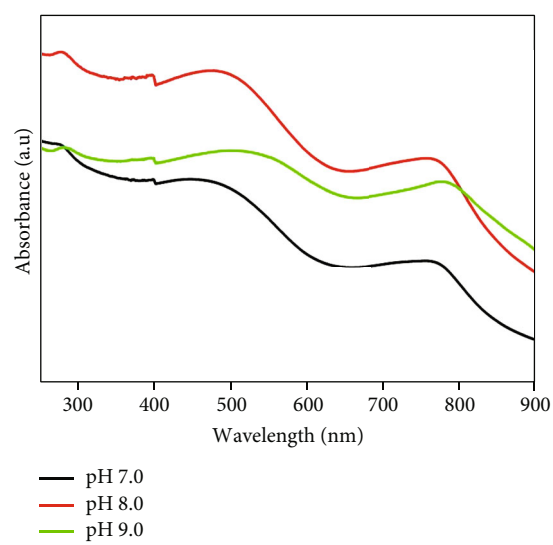

Figure 4: Ultraviolet-visible spectrum of Co_3O_4 nanoparticles.

3.5. Photoluminescence Spectra. The photoluminescence spectra of Co_3O_4 nanomaterials are shown in Figure 6. In Figure 6, it is observed that the intensity of the peaks increased with respect to the alkalinity of the samples (increase in pH). The respective emission peaks observed

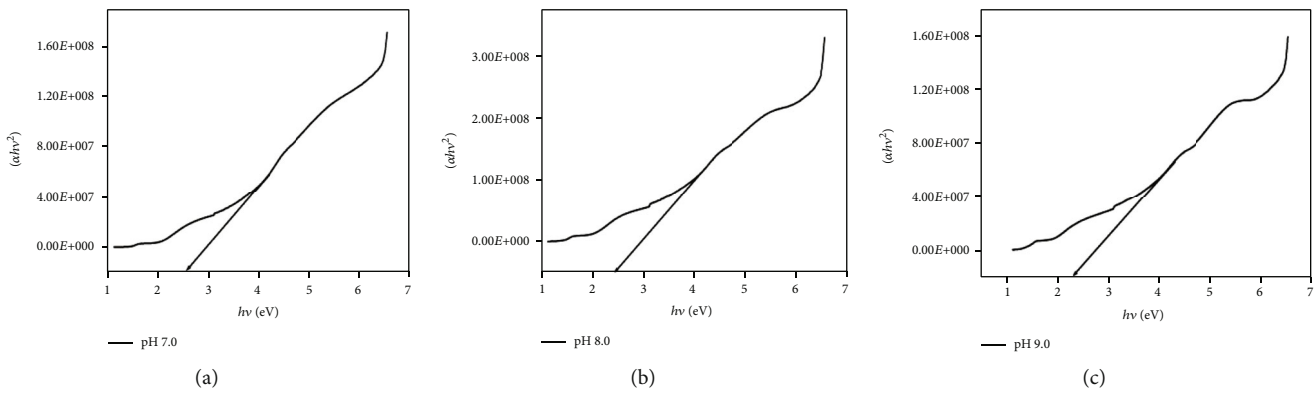

Figure 5: Optical band gap of Co_3O_4 nanomaterials.

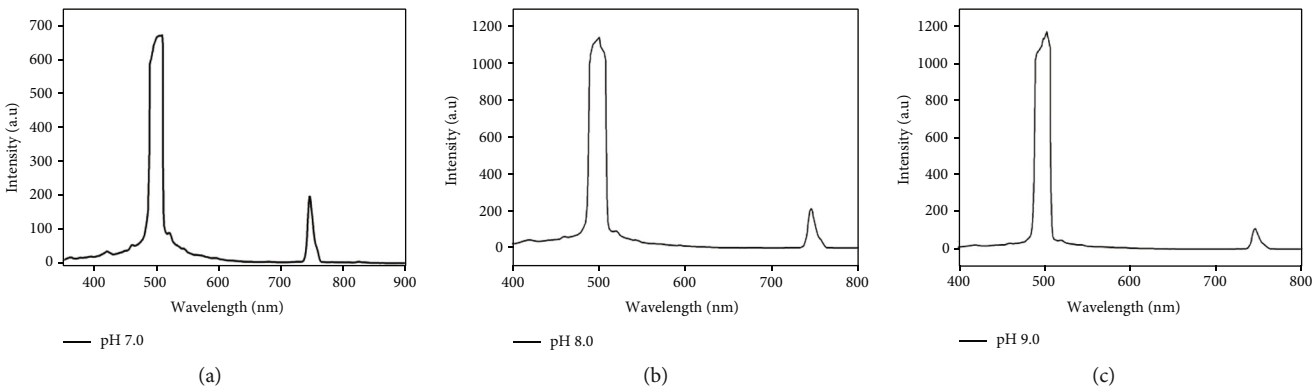

Figure 6: Photoluminescence Spectrum of synthesized Co_3O_4 nanomaterials.

along 488.85 nm, 745 nm, and 488 nm in the spectra are referred to as the deep level emission as it asserts the radiative transition of donors to acceptors [21]. These results indicate that the radiative transition of the donors (cobalt interstitial, oxygen vacancy) to acceptors (cobalt vacancy, oxygen interstitial) is only active at the different pH, concentration etc. of the mother solution. The emission band at 488 nm is represented the interband transition due to the transition between the occupied state of Fermi level and the unoccupied conduction band. It is observed here due to the different particle size [22] and surface morphology [23]. Radial recombination occurs in the surface lattice of Co_3O_4 due to the holes recombining with the electrons found in the singly ionized vacancies of oxygen atoms. So, the luminescence spectra of Co_3O_4 are found to be the presence of the oxygen vacancies in Co_3O_4 nanomaterials [24].

3.6. Magnetic Behaviour. The M-H curve of Co_3O_4 nanomaterials synthesised at various pH is shown in Figure 7. From the curve, it is seen that the prepared particles exhibit paramagnetic behaviour with coercivity value are shown in Table 1. In general, ferromagnetic ordering will be obtained when the excess surface spins present in nanomaterials which may contribute to the weak ferromagnetism in antiferromagnetic materials. In the present work, the prepared samples deliver a weak ferromagnetic behaviour, this may be ascribed to the uncompensated surface spins [25] or the partly inverted spinel structure possibly by local electron hopping [26]. Further, the ferromagnetic behaviour of the

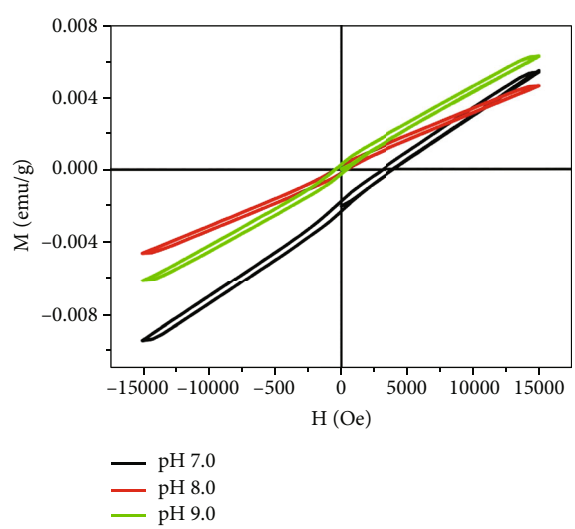

Figure 7: Vibrating sample magnetometry (VSM) spectra of Co_3O_4 nanoparticles.

Table 1: Calculated magnetic parameters of Co_3O_4 nanoparticles at different pH values.

pH	Saturation magnetization, M_s (emu/mg)	Remanence, M_r (emu/mg)	Coercivity, Hc (Oe)	Squareness, M_r/M_s (%)
7.0	5.4511	279.09	407.88	51.199
8.0	4.6175	188.49	428.14	40.820
9.0	6.2530	263.89	423.57	42.202

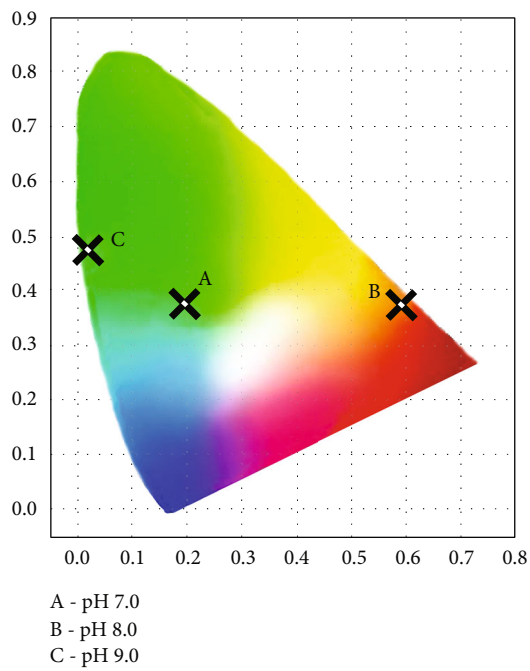

Figure 8: International Commission on Illumination (CIE) colour coordinate diagram of Co_3O_4 for different pH values.

materials relies on defects, oxygen vacancies, and the surface morphology of the nanomaterials. In addition, the fine size of Co_3O_4 particles provides the large surface-to-volume ratio, which favours the magnetic moment from uncompensated surface Co ions. Hence, the observed ferromagnetic nature of Co_3O_4 nanomaterials clearly shows the role of surface spins and surface morphology on the magnetic properties of Co_3O_4 nanomaterials.

3.7. International Commission on Illumination- (CIE-) Chromaticity. The chromaticity coordinates x and y are calculated from the tristimulus values from the following [27].

$$x = \frac{x}{x+y+z}, \quad y = \frac{y}{x+y+z}. \tag{2}$$

Figure 8 shows the CIE-1931 colour coordinate diagram of Co_3O_4 for the pH from 7 to 9. The CIE coordinates (x, y) are found to be (0.196, 0.374), (0.589, 0.373), and (0.018, 0.47) for the materials synthesized at pH 7, 8, and 9. The calculated colour coordinates are listed in Table 2. The cobalt with pH 7 and pH 9 appeared in the green region, whereas the pH 8 sample appeared in the red region. The illumination value of colour tumble emission can be tuned. In order to achieve the white colour, it is required more optimization of the pH value between 7 and 8. The red oxide phosphor-based devices are suffered due to the issues of low colour purity [28]. The CIE coordinates (x, y) for Co_3O_4 with pH 8 are determined to be (0.589, 0.373), as compared to the National Television Standard Committee (NTSC) red (0.67, 0.33). This phosphor has to be tuned for improving colour purity. As depicted, phosphors of Co_3O_4 with different pHs from 7 to 9 could be used as potential emission material, visible light display device, and light-emitting diode applications.

Table 2: CIE-1931 chromaticity coordinates of Co_3O_4 at different pH values.

Sample	X	Y
Cobalt-pH 7	0.196	0.374
Cobalt-pH 8	0.589	0.373
Cobalt-pH 9	0.018	0.47

3.8. Electrochemical Behaviour of Co_3O_4. Figure 9 shows the cyclic voltammetry (CV) curves of the prepared cobalt oxide nanomaterials. The curves show the rectangular type of voltammogram, and this is an indication of notable charge propagation at the electrodes. The shape of the CV does not change while increasing scan rate; the size of the strip only increased which indicates the good charge discharge characteristics with excellent reverse process [29]. This electrochemical study of Co_3O_4 nanomaterials confirms the pseudocapacitive behaviour. The specific capacitance was calculated from CV curves according to the following relation:

$$C_s = \frac{1}{\mathrm{mv}}(V_c - V_a)\int_{v_a}^{v_c} \mathrm{IdV}, \tag{3}$$

where C_s is the specific capacitance (F/g), v is the scan rate (V/s), $(V_c - V_a)$ is potential window, I is the current, and m is the mass (g) of active material.

Figure 10 shows the specific capacitance of the prepared materials. The maximum specific capacitance of 350 F/g was observed, and 1at 0 m/vs at pH-8, 300 F/g was calculated from 300 F/g and 275 F/g found for pH-7 only. However, the material prepared at pH-8 only has high specific capacitance because their well-defined cubic shape [14]. Figure 11 shows electrochemical impedance

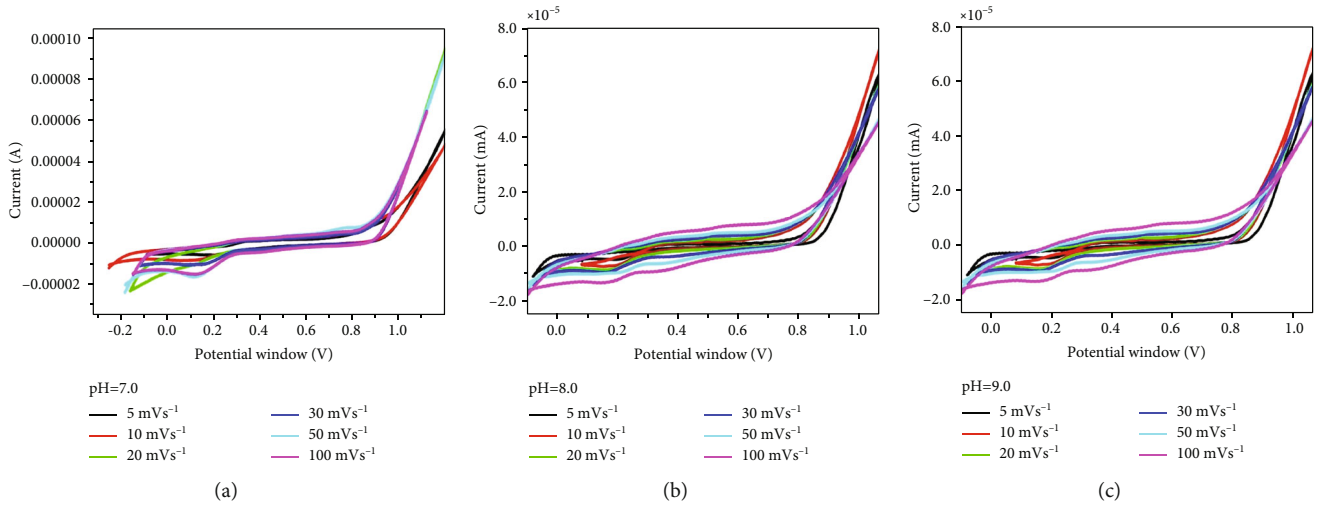

Figure 9: CV curve of Co_3O_4 nanoparticles (a) at pH 7.0, (b) at pH 8.0, and (c) at pH 9.0.

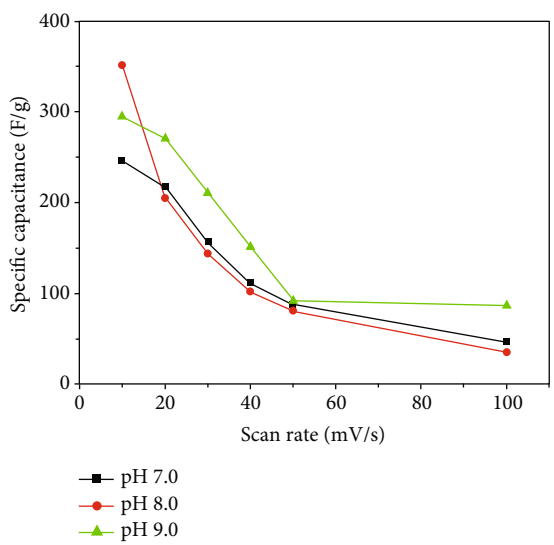

Figure 10: The specific capacitance of Co_3O_4 nanomaterials in various scan rate and in different pH.

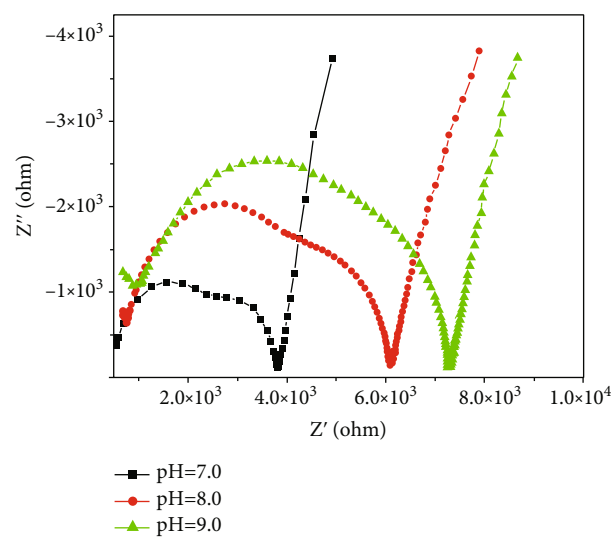

Figure 11: Electrochemical impedance spectroscopy of Co_3O_4 nanoparticles at different pH values.

spectroscopy of Co_3O_4 nanoparticles at different pH values. The Nyquist plots of Co_3O_4 nanomaterials have a semicircle in the high-frequency region and a vertical line in the low-frequency region. In the high-frequency region, the semicircle belongs to the charge transfer process, and in the low range frequency shows the vertical line is the Warburg impedance plot of the high capacitive behaviour of the rapid ions.

4. Conclusions

The Co_3O_4 nanomaterials were prepared by coprecipitation by maintaining the pH of the reaction solution at 7, 8, and 9. The XRD pattern showed cubic spinel structure, and the calculated crystal size ranges from 14 to 10 nm when the pH changes from 7 to 9. The variation in morphology of Co_3O_4 nanomaterials was investigated by SEM. The CV curves indicate a rectangular type of voltammogram, signifying good charge propagation with the electrodes. The optical absorption band gaps of Co_3O_4 nanomaterials were estimated at 2.5, 2.4, and 2.2 eV for pH 7, 8, and 9, respectively. The emission band at 488 nm is attributed to the transition taking place here; the size effect and surface morphology were observed in the XRD and SEM. The VSM studies show that the synthesized nanomaterials exhibit weak ferromagnetism in antiferromagnetic nature. This work concluded that the tunable properties such as particle size and band gap of Co_3O_4 nanomaterials were achieved under different pH conditions. Also, the primary studies proved that the prepared Co_3O_4 nanomaterials could serve as photoluminescence applications.

Data Availability

All materials for this study are presented in this article and available on request to the corresponding author.

Conflicts of Interest

The authors declare that they have no conflicts of interest.

Authors' Contributions

Conceptualization, methodology, and supervision were done by KJ, PAV, and PK. Investigation and validation were performed by VR, MM, and SM. Validation and data curation were conducted by PK and PAV. Resources and data curation were assigned to GP, PK, and MS. Writing, which is the original draft preparation, was done by KJ, GP, VR, and SKS. Writing, which includes reviewing and editing, was performed by GP, MM, and GG. Project administration was conducted by PK, PAV, and GG. All authors have read and agreed to the published version of the manuscript.

Acknowledgments

The authors convey their heartfelt gratitude to the management of SRM IST for their motivation and support. The project was supported by the Researchers Supporting Project number (RSPD2023R675), King Saud University, Riyadh, Saudi Arabia. We thank the DST-SERB (EMR/2016/000055), India, for the financial support of this research.

References

[1] C. S. Kumar, *Semiconductor Nanomaterials*, John Wiley & Sons, 2010.

[2] P. Ball and L. Garwin, "Science at the atomic scale," *Nature*, vol. 355, no. 6363, pp. 761–764, 1992.

[3] R. Cavicchi and R. Silsbee, "Coulomb suppression of tunneling rate from small metal particles," *Physical Review Letters*, vol. 52, no. 16, pp. 1453–1456, 1984.

[4] W.-Y. Li, L.-N. Xu, and J. Chen, "Co_3O_4 nanomaterials in lithium-ion batteries and gas sensors," *Advanced Functional Materials*, vol. 15, no. 5, pp. 851–857, 2005.

[5] M. Salavati-Niasari, A. Khansari, and F. Davar, "Synthesis and characterization of cobalt oxide nanoparticles by thermal treatment process," *Inorganica Chimica Acta*, vol. 362, no. 14, pp. 4937–4942, 2009.

[6] X. Liu, G. Qiu, and X. Li, "Shape-controlled synthesis and properties of uniform spinel cobalt oxide nanocubes," *Nanotechnology*, vol. 16, no. 12, pp. 3035–3040, 2005.

[7] Z.-Y. Li, P. T. Bui, D.-H. Kwak, M. S. Akhtar, and O.-B. Yang, "Enhanced electrochemical activity of low temperature solution process synthesized Co_3O_4 nanoparticles for pseudo-supercapacitors applications," *Ceramics International*, vol. 42, no. 1, pp. 1879–1885, 2016.

[8] Y. Dong, K. He, L. Yin, and A. Zhang, "A facile route to controlled synthesis of Co_3O_4 nanoparticles and their environmental catalytic properties," *Nanotechnology*, vol. 18, no. 43, article 435602, 2007.

[9] M. Malligavathy and D. Pathinettam Padiyan, "Role of pH in the hydrothermal synthesis of phase pure alpha Bi2O3 nanoparticles and its structural characterization," *Advanced Materials Proceedings*, vol. 2, no. 1, pp. 51–55, 2021.

[10] E. Albanese, A. Ruiz Puigdollers, and G. Pacchioni, "Theory of ferromagnetism in reduced ZrO2–xnanoparticles," *ACS Omega*, vol. 3, no. 5, pp. 5301–5307, 2018.

[11] V. Ratchagar and K. Jagannathan, "Effect of pH on magnetic, thermal and dielectric properties of SnO_2 nanomaterials," *Journal of Alloys and Compounds*, vol. 689, pp. 1088–1095, 2016.

[12] N. Baig, I. Kammakakam, and W. Falath, "Nanomaterials: a review of synthesis methods, properties, recent progress, and challenges," *Materials Advances*, vol. 2, no. 6, pp. 1821–1871, 2021.

[13] M. R. S. A. Janjua, "Synthesis of Co_3O_4 nano aggregates by co-precipitation method and its catalytic and fuel additive applications," *Open Chemistry*, vol. 17, no. 1, pp. 865–873, 2019.

[14] J. Feng and H. C. Zeng, "Size-controlled growth of Co_3O_4 nanocubes," *Chemistry of Materials*, vol. 15, no. 14, pp. 2829–2835, 2003.

[15] S.-H. Wu and D.-H. Chen, "Synthesis and characterization of nickel nanoparticles by hydrazine reduction in ethylene glycol," *Journal of Colloid and Interface Science*, vol. 259, no. 2, pp. 282–286, 2003.

[16] S. Thota, A. Kumar, and J. Kumar, "Optical, electrical and magnetic properties of Co_3O_4 nanocrystallites obtained by thermal decomposition of sol-gel derived oxalates," *Materials Science and Engineering: B*, vol. 164, no. 1, pp. 30–37, 2009.

[17] D. Anggraini, P. K. Wardani, M. Agustina, A. Awaluddin, and K. Arifin, "Tio_2/Co_3O_4 composite as photoanode of photoelectrochemical water splitting," *Journal of Physics: Conference Series*, vol. 1351, no. 1, article 012032, 2019.

[18] C. T. Anuradha and P. Raji, "Facile synthesis and characterization of Co_3O_4 nanoparticles for high-performance supercapacitors using *Camellia sinensis*," *Applied Physics A*, vol. 126, no. 3, p. 164, 2020.

[19] T. He, D. Chen, X. Jiao, Y. Wang, and Y. Duan, "Solubility-controlled synthesis of high-quality Co_3O_4 Nanocrystals," *Chemistry of Materials*, vol. 17, no. 15, pp. 4023–4030, 2005.

[20] A. B. Vennela, D. Mangalaraj, N. Muthukumarasamy, S. Agilan, and K. V. Hemalatha, "Structural and optical properties of Co_3O_4 nanoparticles prepared by sol-gel technique for photocatalytic application," *International Journal of Electrochemical Science*, vol. 14, pp. 3535–3552, 2019.

[21] I. P. Koziarskyi, E. V. Maistruk, D. P. Koziarskyi, and P. D. Maryanchuk, *Optical Properties of Cobalt Oxide Thin Films*, 2020 IEEE 10th International Conference Nanomaterials: Applications & Properties (NAP), 2020.

[22] P. Chand, A. Gaur, and A. Kumar, "Structural, optical and ferroelectric behavior of CuO nanostructures synthesized at different pH values," *Superlattices and Microstructures*, vol. 60, pp. 129–138, 2013.

[23] R. Al-Tuwirqi, A. A. Al-Ghamdi, N. A. Aal, A. Umar, and W. E. Mahmoud, "Facile synthesis and optical properties of Co_3O_4 nanostructures by the microwave route," *Superlattices and Microstructures*, vol. 49, no. 4, pp. 416–421, 2011.

[24] C. Ramamoorthy and V. Rajendran, "Effect of surfactants assisted Co_3O_4 nanoparticles and its structural, optical, magnetic and electrochemical properties," *Optik*, vol. 145, pp. 330–335, 2017.

[25] A. M. Amanulla, S. J. Shahina, R. Sundaram et al., "Antibacterial, magnetic, optical and humidity sensor studies of β-$CoMoO_4$ - Co_3O_4 nanocomposites and its synthesis and characterization," *Journal of Photochemistry and Photobiology B: Biology*, vol. 183, pp. 233–241, 2018.

[26] H. Zhu, J. Luo, J. Liang et al., "Synthesis and magnetic properties of antiferromagnetic Co_3O_4 nanoparticles," *Physica B: Condensed Matter*, vol. 403, no. 18, pp. 3141–3145, 2008.

[27] T. Ozkaya, A. Baykal, Y. Koseoğlu, and H. Kavas, "Synthesis of Co_3O_4 nanoparticles by oxidation-reduction method and its magnetic characterization," *Open Chemistry*, vol. 7, no. 3, pp. 410–414, 2009.

[28] B. Shanmugavelu and V. R. K. Kumar, "Luminescence studies of Dy^{3+} doped bismuth zinc borate glasses," *Journal of Luminescence*, vol. 146, pp. 358–363, 2014.

[29] W.-W. Liu, W.-M. Lau, and Y. Zhang, "The electrochemical properties of Co_3O_4 as a lithium-ion battery electrode: a first-principles study," *Physical Chemistry Chemical Physics*, vol. 20, no. 38, pp. 25016–25022, 2018.